Available online at www.sciencedirect.com
ScienceDirect
Journal of Solid State Chemistry 180 (2007) 1353–1364
JOURNAL OF SOLID STATE CHEMISTRY
www.elsevier.com/locate/jssc

Single crystal X-ray diffraction study of a mixed-valence gold compound, $Cs_2Au^IAu^{III}Cl_6$ under high pressures up to 18 GPa: Pressure-induced phase transition coupled with gold valence transition

Nobuyuki Matsushita[a,b,*,1], Hans Ahsbahs[a], Stefan S. Hafner[a], Norimichi Kojima[b]

[a]*Institute of Mineralogy, University of Marburg, Marburg 35032, Germany*
[b]*Department of Basic Science, Graduate School of Arts and Sciences, The University of Tokyo, Komaba, Meguro-ku, Tokyo 153-8902, Japan*

Received 29 November 2006; received in revised form 16 January 2007; accepted 23 January 2007
Available online 15 February 2007

Abstract

We performed the single-crystal X-ray diffraction study of a perovskite-type gold mixed-valence compound, $Cs_2Au^IAu^{III}Cl_6$, under high pressures up to 18 GPa by using a diamond-anvil-cell with helium gas as an ideal hydrostatic pressure-transmitting medium. The lattice parameters and the variable atomic positional parameters were obtained with reasonable accuracy at various pressures. A structural phase transition at ca. 12.5 GPa from $I4/mmm$ to $Pm3m$ was found. The lattice parameters a_0 and c_0, denoted in the tetragonal cell setting, result in the relationship $2^{1/2}a_0 = c_0$, and the superstructure reflections $h\,k\,l$ (l is odd), caused by the shift of the Cl ions from the midpoint of the Au ions, disappeared at pressures above the phase transition. Both elongated $[Au^{III}Cl_6]$ and compressed $[Au^ICl_6]$ octahedra in the low-pressure phase smoothly approach regular octahedra with increasing pressure. Above the structural phase transition at 12.5 GPa, all the $[AuCl_6]$ octahedra are crystallographically equivalent, which shows that the tetragonal-to-cubic phase transition accompanies the valence transition from the Au^I/Au^{III} mixed-valence state to the Au^{II} single-valence state.

Keywords: Chloro-bridged gold complex; Mixed-valence compound; Perovskite-type structure; High pressure structure analysis; Single-crystal X-ray diffraction; Phase transitions; Valence transition; Diamond-anvil-cell; Helium pressure medium

1. Introduction

Mixed-valence compounds with perovskite-type structures have attracted much interest in view of high-T_c superconductors such as $La_{2-x}Ba_xCuO_4$ [1] and $Ba_{1-x}K_xBiO_3$ [2]. In these systems, interesting physical properties such as superconductivity remarkably depend on the valence state. An interesting group of mixed-valence perovskites is halogen-bridged gold mixed-valence complexes, $Cs_2Au_2X_6$ (X = Cl, Br, and I), which are typical mixed-valence compounds belonging to class II in the classification of mixed-valence compounds of Robin and Day [3], and which consist of univalent Au^I and trivalent Au^{III} linked by halide ions in all three dimensions. Their structures are generally of tetragonal symmetry at ambient conditions. As shown in Fig. 1, they comprise elongated $[Au^{III}X_6]$ octahedra and compressed $[Au^IX_6]$ octahedra, sharing corners. The question arises how the valence states of Au associated with polyhedral distortion may change with increasing pressure. In addition, the question that an ideally cubic perovskite structure with divalent Au^{II} may be adopted above a critical pressure also arises. In consequence of these questions for the electronic properties and the phase transition at high pressures, $Cs_2Au_2X_6$ (X = Cl, Br, and I) have received much attention. So far, various techniques have been employed to study these complexes as follows: single-crystal X-ray diffraction both under ambient conditions [4–6] and at high pressures [7,8], high-pressure powder X-ray diffraction with Rietveld/MEM analysis [9], high-pressure energy dispersive X-ray

*Corresponding author. Department of Basic Science, Graduate School of Arts and Sciences, The University of Tokyo, Komaba, Meguro-ku, Tokyo 153-8902, Japan. Fax: +81 3 5454 6571.
E-mail address: cnmatsu@mail.ecc.u-tokyo.ac.jp (N. Matsushita).
[1]Present address: The University of Tokyo.

0022-4596/$ - see front matter © 2007 Elsevier Inc. All rights reserved.
doi:10.1016/j.jssc.2007.01.037

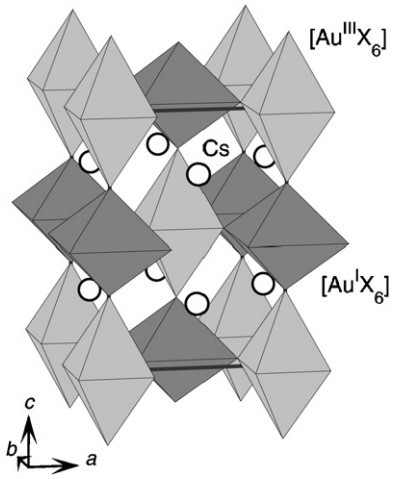

Fig. 1. The crystal structure of the perovskite-type halides, $Cs_2Au^IAu^{III}X_6$ (X = Cl, Br, I).

diffraction [10,11], high-pressure neutron diffraction [12], pressure-dependence of conductivity [13–18], ^{197}Au Mössbauer spectroscopy both at atmospheric pressure [19–21] and at high pressures [22–24], optical spectroscopy [25,26], Raman spectroscopy under high pressures [27–29], X-ray absorption spectroscopy at Au L_{III} edge [30], X-ray photoelectron spectroscopy [31], ESR [32], band structure calculations [33–35], anomalous scattering diffraction with Au L_{III} absorption edge [36].

In 1990s, the high-pressure behavior of $Cs_2Au_2I_6$ has been explored in more detail than those of $Cs_2Au_2X_6$ (X = Cl and Br). Kojima, Kitagawa et al. reported a semiconductor-to-metal transition (tetragonal to tetragonal) at about 5 GPa and room temperature and a further metal-to-metal transition (tetragonal to cubic) at about 6.5 GPa and 350 K [11,14]. Remarkably, the cubic phase appearing at high-pressure and above room temperature is metastable even at ambient pressure and room temperature [14]. ^{197}Au Mössbauer study on the quenched material indicates the presence of a single Au site in the cubic phase [21]. ^{197}Au Mössbauer spectroscopic measurement at high-pressures shows that the difference of Mössbauer parameters between the two Au sites decreases with increasing pressure, and that there is only one Au site of Au^{II} at 12.5 GPa [22]. The Au sites become equivalent somewhere between 6.6 and 12.5 GPa. In 2000s, the pressure-induced Au valence transition from the Au^I/Au^{III} mixed-valence state to the Au^{II} single-valence one has been investigated by means of Raman spectroscopy. According to the Raman spectroscopic study, $Cs_2Au_2X_6$ (X = Cl and Br) undergo the Au valence transition at about 12.2 and 7.5 GPa, respectively [28]. Sakata et al. have estimated the charge densities of the Au sites in $Cs_2Au_2Br_6$ by Rietveld/MEM analysis with high-pressure X-ray powder diffraction and confirmed the Au valence transition around 8 GPa for $Cs_2Au_2Br_6$ [9]. As a remarkable topic, Liu et al. have discovered a photo-induced Au valence transition for $Cs_2Au_2Br_6$ at pressures between 6.4 and 6.8 GPa [29]. These characteristic properties of $Cs_2Au_2X_6$ (X = Cl, Br, and I) have been reviewed in Refs. [37,38].

Turning to $Cs_2Au_2Cl_6$, the resistivity at room temperature drops by nine orders of magnitude from ambient pressure to 10 GPa, and a change in electrical behavior from semiconducting to metallic occurs at around 6 GPa [13]. The single-crystal X-ray diffraction study of $Cs_2Au_2Cl_6$ at pressures up to 5.2 GPa [7] has shown that the decrease of the resistivity is associated with the displacement of the bridging Cl ions toward the midpoints between adjacent Au sites with increasing pressure. At about 5.2 GPa, the Au sites attain crystallographically equivalent, suggesting a nominal valence state of Au^{II}, but the structure is still tetragonal by the single-crystal X-ray diffraction. ^{197}Au Mössbauer spectroscopy up to 6.8 GPa [23,24] and Raman spectroscopy up to 8 GPa [27], however, suggest that there are still two distinct Au sites in the compound up to each pressure. In addition, according to the recent high-pressure Raman spectroscopy [28], $Cs_2Au_2Cl_6$ undergoes the Au valence transition from the Au^I/Au^{III} mixed-valence state to the Au^{II} single-valence one at about 12.2 GPa.

The single-crystal X-ray diffraction analysis is the most powerful method to clarify the existence of a phase transition to a cubic structure with equivalent Au sites at high pressures, coupled with the Au valence transition, and to quantitatively evaluate the displacement of the bridging Cl ions distorted from the midpoints between adjacent Au sites as a function of pressure. Here, we report in detail the single-crystal X-ray diffraction study of $Cs_2Au_2Cl_6$, under high pressures up to 18 GPa by using a diamond-anvil-cell with helium gas as an ideal hydrostatic pressure-transmitting medium. Preliminary results of the present study have been reported [8].

2. Experimental procedure

2.1. Preparation of single crystals

Single crystals of $Cs_2Au_2Cl_6$ were recrystallized by a diffusion method, using an H-type glass test tube and hydrochloric acid as the solvent [25]. One leg of the H-tube with the original crystals was kept at 45 °C. Recrystallized crystals grew at the other leg kept at 20 °C. Single crystals suitable for X-ray crystallography were obtained in a few weeks. Two plate-like crystals with dimensions of $65 \times 77 \times 24\,\mu m^3$ (crystal 1) and $89 \times 116 \times 25\,\mu m^3$ (crystal 2) were selected for the X-ray diffraction measurements at high pressures. The plate of crystal 1 was parallel to (010) whereas that of crystal 2 was parallel to (110), which was confirmed by photographs taken with a precession camera. Very thin plate-like crystals were transparent and showed a remarkable dichroism with red color for the polarized light parallel to the c-axis and with opaqueness for the polarized light perpendicular to the c-axis. The dichroism is due to the highly anisotropic intervalence charge–transfer

interaction between the Au^{I} and Au^{III} ions indicated by Kojima and Kitagawa [25].

2.2. High-pressure technique

As an apparatus generating high pressure, we used a Merill–Bassett-type diamond-anvil-cell having four screws [39,40], which was modified by Ahsbahs [41]. The cell was equipped with 600 μm culet diamonds. Thyrodur 2709 steel (THYSSEN) was used as a gasket. The gasket was preindented to thickness of about 60 μm, and drilled a hole of 400 μm, and then, hardened at 500 °C putting in a closed vessel full of iron powder [42]. The $Cs_2Au_2Cl_6$ crystal was loaded into the hole of the gasket in the diamond-anvil-cell with two or three small (ca. 25 μm) ruby chips for pressure calibration and He gas was loaded in an autoclave at 0.2 GPa as an inert and hydrostatic pressure-transmitting medium. Pressure was measured before and after each X-ray diffraction measurement using the ruby fluorescence method. The error of the pressure measurement was estimated at 0.05 GPa.

X-ray diffraction data for the unit-cell parameters were measured at 0.69, 2.43, 3.11 and 4.45 GPa with the crystal 1, and at eighteen pressure points with the crystal 2. The X-ray intensity data were collected at 0.69, 2.43 and 4.45 GPa with the crystal 1, and at ambient pressure, 4.56, 6.09, 7.47, 9.47, 11.25, 12.23 and 15.00 GPa with the crystal 2.[2]

2.3. X-ray diffraction

X-ray diffraction measurements were performed on an STOE automated four-circle diffractometer with graphite-monochromated Mo$K\alpha$ radiation (0.71073 Å). The measurement at ambient pressure was also carried out in the diamond-anvil-cell. The diffractometer was used on fixed [43] from the geometrical restriction of diamond-anvil-cell. The unit-cell parameters were determined by using 14–16 reflections. Each reflection was centered in eight positions by using the method of King and Finger [44] to reduce deviations in the position of a crystal from the center of alignment of a goniometer and a diffractometer. The precise lattice parameters were calculated using a least-square refinement program in a software package for structural analysis *CRYMIS* [45]. Crystal data are shown in Table 1.

The intensity data of X-ray diffraction were collected with ω scans technique and a step scan mode in two categories with regards to the reflections. One is a group of main reflections, which are based on the framework of the simple perovskite lattice. The other is a group of superstructure reflections, which are caused by the deviation of the Cl atoms from the midpoint between the Au atoms. The intensity data of X-ray diffraction were measured with different scan rates for the main reflections and the superstructure reflections. Two standard reflections, 2 2 0 and 0 0 4, were monitored at intervals of 300 min during the measurement for the main reflections and every 20 reflections for the superstructure reflections. No intensity decay was observed for the standard reflections.

The diamond-anvil-cell produces a blind region in a reciprocal lattice for measuring the intensity data of X-ray diffraction. The measurable region in the case of using the present diamond-anvil-cell is 32.5% of that without the cell for $2\theta_{max} = 65^{\circ}$ and Mo$K\alpha$ radiation. In the present measurements, the plates of the two crystals used as mentioned in Section 2.1 were paralleled to the surface of the diamond. The measurements gave the number of the independent reflections more than 10 times of that of the variable parameters in the refinement of the structure with isotropic displacement parameters. The independent all reflections measured were used in the refinement at each pressure. However, the ratio of the number of the reflections used in the refinement to that of all independent reflections for $2\theta_{max} = 65^{\circ}$ and Mo$K\alpha$ radiation is 40–50% in the low-pressure phase of $I4/mmm$. The ratio in the high-pressure phase of $Pm3m$ is about 70%, and that in the metastable state of $P4/mmm$ is about 60%. In using such a high-pressure cell, it is very difficult to make a measurement in which the ratio, the so-called completeness, is more than 80%.

A specially designed collimator [46,47] was mounted at the diffracted beam side of the diamond-anvil-cell to reduce the background scattered mainly by the beryllium backing plates of the diamond-anvil-cell. For measuring the absorption caused by the diamond anvils and the beryllium plates, a primary collimator with a diameter of 0.15 mm was used. The diameter of this beam was similar to that of the diffracted beams defined by the size of the crystal in the procedure of the intensity data collection. For measuring the absorption, this small-sized incident beam was adjusted to the center of the diamond culets of an empty cell without gasket. The measured intensities were analytically corrected based on the absorption factor depending on the tilting angle of the diamond-anvil-cell. The intensity data were integrated from the profile data of the step scan, corrected for the absorption of the diamond anvils and of the beryllium plates, and for Lorentz-polarization factor.

The programs used were *DIF*4 [48] modified for high-pressure data collection, *MDIF*4 [49], and *PROFILE* [50] for data reduction and the absorption correction of the diamond anvils and of the beryllium plates. Information of the data collection is summarized in Table 1.

[2]The crystal 1 was fixed on a surface of the diamond with using a little amount of vaseline as glue. With increasing pressure, the reflection peaks were split little by little into two parts in ω without broadening. The splitting of peaks disappeared at ambient pressure after releasing pressure. This mechanical splitting could be produced by a shear stress due to the different compressibilities of the crystal and the glue. To avoid the splitting, then, the crystal 2 was put on a surface of the diamond without glue. Without the mechanical splitting of reflections, we measured the unit-cell parameters and collected the X-ray intensity data.

Table 1
Crystal data and experimental summary

P		10^{-4} GPa	0.69 GPa	2.43 GPa	4.45 GPa	4.56 GPa	6.09 GPa
Crystal data							
Chemical formula		$Cs_2Au_2Cl_6$	$Cs_2Au_2Cl_6$	$Cs_2Au_2Cl_6$	$Cs_2Au_2Cl_6$	$Cs_2Au_2Cl_6$	$Cs_2Au_2Cl_6$
Cell setting		Tetragonal	Tetragonal	Tetragonal	Tetragonal	Tetragonal	Tetragonal
Space group		*I*4/*mmm*	*I*4/*mmm*	*I*4/*mmm*	*I*4/*mmm*	*I*4/*mmm*	*I*4/*mmm*
a(Å)		7.5004(8)	7.3948(6)	7.2072(7)	7.0629(9)	7.0646(6)	6.9933(7)
c (Å)		10.8836(7)	10.7532(12)	10.5060(15)	10.3000(10)	10.2982(8)	10.1851(8)
V (Å^3)		612.28(12)	588.02(11)	545.73(13)	513.82(13)	513.97(10)	498.11(10)
Z		2	2	2	2	2	2
Dx (mg/m^3)		4.73	4.93	5.31	5.64	5.64	5.82
Data collection							
Reflections measured		368	408	357	312	324	324
Reflections unique		119	149	134	126	116	114
Reflections [$F_o > 4\sigma(F_o)$]		95	102	89	88	97	90
R_{int}		0.0300	0.0809	0.0464	0.0933	0.0565	0.0442
θ_{max} (deg)		29.96	30.31	31.13	30.87	31.44	31.47
Index range	*h*	−6 to 8	−6 to 10	−6 to 10	−6 to 10	−6 to 7	−6 to 7
	k	−7 to 8	−2 to 3	−2 to 2	−2 to 2	−6 to 8	−6 to 8
	l	−9 to 14	−11 to 14	−11 to 14	−10 to 14	−8 to 14	−8 to 14
Refinement							
Refinement on		F^2	F^2	F^2	F^2	F^2	F^2
R [$F_o > 4\sigma(F_o)$]		0.0379	0.0383	0.0365	0.0573	0.0275	0.0275
wR		0.0912	0.0786	0.0893	0.1089	0.0283	0.0125
S		0.937	0.795	0.763	1.405	0.686	0.566
No. of reflections used in refinement		119	149	134	126	116	114
No. of parameters used		9	9	9	9	9	9
Weighting scheme ($P = (F_o^2 + 2F_c^2)/3$)		$w = [\sigma^2(F_o) + (0.0200P)^2]^{-1}$	$w = [\sigma^2(F_o) + (0.0119P)^2]^{-1}$	$w = [\sigma^2(F_o) + (0.0240P)^2]^{-1}$	$w = [\sigma^2(F_o) + (0.0164P)^2]^{-1}$	$w = [\sigma^2(F_o) + (0.0035P)^2]^{-1}$	$w = [\sigma^2(F_o) + (0.0006P)^2]^{-1}$
Extinction coefficient[a]		0.0026(4)	0.0021(4)	0.0014(3)	0.0032(5)	0.0014(1)	0.0022(2)

P		7.47 GPa	9.47 GPa	11.25 GPa	15.00 GPa	12.23 GPa
Crystal data						
Chemical formula		$Cs_2Au_2Cl_6$	$Cs_2Au_2Cl_6$	$Cs_2Au_2Cl_6$	$CsAuCl_3$	$CsAuCl_3$
Cell setting		Tetragonal	Tetragonal	Tetragonal	Cubic	Tetragonal
Space group		*I*4/*mmm*	*I*4/*mmm*	*I*4/*mmm*	*Pm*3*m*	*P*4/*mmm*
a (Å)		6.9359(6)	6.8671(7)	6.8204(6)	4.7694(3)	4.8196(8)
c (Å)		10.0877(8)	9.8856(8)	9.7408(7)		4.8293(8)
V (Å^3)		485.27(9)	466.17(9)	453.13(8)	108.49(2)	112.18(4)
Z		2	2	2	1	1
Dx (mg/m^3)		5.97	6.22	6.40	6.68	6.46
Data collection						
Reflections measured		299	258	278	221	231
Reflections unique		107	100	109	47	94
Reflections [$F_o > 4\sigma(F_o)$]		95	76	85	41	76
R_{int}		0.0492	0.0553	0.0504	0.0458	0.0439
θ_{max} (deg)		31.28	31.50	32.46	32.85	32.80
Index range	*h*	−6 to 7	−6 to 7	−6 to 7	−5 to 7	−5 to 7
	k	−6 to 8	−6 to 8	−6 to 8	−1 to 1	−1 to 1
	l	−8 to 14	−8 to 14	−8 to 14	−4 to 7	−4 to 7
Refinement						
Refinement on		F^2	F^2	F^2	F^2	F^2
R [$F_o > 4\sigma(F_o)$]		0.0262	0.0348	0.0290	0.0195	0.0253
wR		0.0497	0.0686	0.0574	0.0379	0.0465
S		0.778	0.911	0.833	0.763	0.655
No. of reflections used in refinement		107	100	109	47	94
No. of parameters used		9	9	9	5	6
Weighting scheme ($P = (F_o^2 + 2F_c^2)/3$)		$w = [\sigma^2(F_o) + (0.0006P)^2]^{-1}$	$w = [\sigma^2(F_o) + (0.0139P)^2]^{-1}$	$w = [\sigma^2(F_o) + (0.0091P)^2]^{-1}$	$w = [\sigma^2(F_o) + (0.0100P)^2]^{-1}$	$w = [\sigma^2(F_o) + (0.0127P)^2]^{-1}$
Extinction coefficient[a]		0.0022(2)	0.0013(2)	0.0029(3)	0.011(3)	0.006(2)

[a]Method: *SHELXL* 93.

2.4. Refinement

The initial atomic positional parameters for the tetragonal phase (*I*4/*mmm*) below a phase transition at ca. 12.5 GPa were obtained from previous report [4]. We solved and refined the structure at 15.00 GPa based on cubic, *Pm*3*m* above the phase transition and that at 12.23 GPa based on tetragonal, *P*4/*mmm* as a metastable state in the path of descendant pressure within the region of pressure hysteresis (see Section 3.4).

The structures were refined on F^2 by full matrix least-squares method with isotropic displacement parameters. The refinement information is summarized in Table 1. The atomic positional and isotropic displacement parameters are listed in Table 2. Programs used were *SHELXL*93 [51] for the refinement, the extinction correction and the averaging procedure of the reflections, and *DIAMOND* [52] for drawing.

Further details of the crystal structure investigations can be obtained from the Fachinformationszentrum Karlsruhe, 76344 Eggenstein-Leopoldshafen, Germany (fax: (+49) 7247-808-666; e-mail: crysdata@fiz.karlsruhe.de, http://www.fiz-karlsruhe.de/ecid/Internet/en/DB/icsd/depot_anforderung.html) on quoting the depository numbers CSD-417363 (10^{-4} GPa), -417364 (0.69 GPa), -417365 (2.43 GPa), -417366 (4.45 GPa), -417367 (4.56 GPa), -417368 (6.09 GPa), -417369 (7.47 GPa), -417370 (9.47 GPa), -417371 (11.25 GPa), -417372 (15.00 GPa), and -417373 (12.23 GPa).

2.5. Hydrostatic pressure

The two crystals kept their diffraction qualities over the entire paths of ascending and descending pressures. This is demonstrated by the intensity profiles of reflection 0 0 4 shown in Fig. 2. The light broadening at 12.2 GPa may be due to transition hysteresis. Returned to ambient condition after the high-pressure experiment, the crystals yielded original diffraction quality. We interpret this behavior also as sign of highly hydrostatic pressures even at the highest pressures, as expected from the He pressure media used.

Table 2
Atomic positional parameters and isotropic displacement parameters (Å^2) at various pressures

(a) *Tetragonal I4/mmm in the low-pressure phase*

P/GPa	Au(1)[a]	Au(2)[b]	Cs[c]	Cl(1)[d]		Cl(2)[e]	
	$U_{iso.}$	$U_{iso.}$	$U_{iso.}$	$x(=y)$	$U_{iso.}$	z	$U_{iso.}$
10^{-4}(a.p.)	0.0229(10)	0.0256(10)	0.0447(13)	0.2143(13)	0.044(3)	0.2082(14)	0.039(4)
0.69	0.0195(10)	0.0212(10)	0.0384(13)	0.2201(12)	0.037(2)	0.2124(14)	0.034(4)
2.43	0.0167(9)	0.0150(8)	0.0280(9)	0.2253(10)	0.027(2)	0.2155(12)	0.026(3)
4.45	0.0152(17)	0.0118(16)	0.0250(12)	0.2309(18)	0.022(4)	0.2207(16)	0.018(5)
4.56	0.0117(5)	0.0127(5)	0.0233(6)	0.2300(7)	0.0219(16)	0.2205(7)	0.026(2)
6.09	0.0110(5)	0.0116(5)	0.0197(6)	0.2328(6)	0.0192(16)	0.2241(7)	0.021(2)
7.47	0.0107(5)	0.0114(5)	0.0179(5)	0.2351(7)	0.0184(15)	0.2282(7)	0.020(2)
9.47	0.0089(11)	0.0104(11)	0.0174(8)	0.2419(17)	0.018(2)	0.2356(19)	0.026(4)
11.25	0.0088(8)	0.0087(8)	0.0160(6)	0.2435(14)	0.015(2)	0.2401(14)	0.018(3)

(b) *Cubic Pm3m at 15.00 GPa in the high-pressure phase*

Atom	x	y	z	$U_{iso.}$
Au	0	0	0	0.0086(4)
Cs	1/2	1/2	1/2	0.0131(5)
Cl	1/2	0	0	0.0123(14)

(c) *Tetragonal P4/mmm at 12.23 GPa in the metastable state in the path of descendant pressure within the region of pressure hysteresis*

Atom	x	y	z	$U_{iso.}$
Au	0	0	0	0.0099(4)
Cs	1/2	1/2	1/2	0.0156(5)
Cl(1)	1/2	0	0	0.0161(13)
Cl(2)	0	0	1/2	0.0165(17)

[a] $x = y = z = 0$ for Au(1).
[b] $x = y = 1/2$, $z = 0$ for Au(2).
[c] $x = 0$, $y = 1/2$, $z = 1/4$ for Cs.
[d] $z = 0$ for Cl(1).
[e] $x = y = 1/2$ for Cl(2).

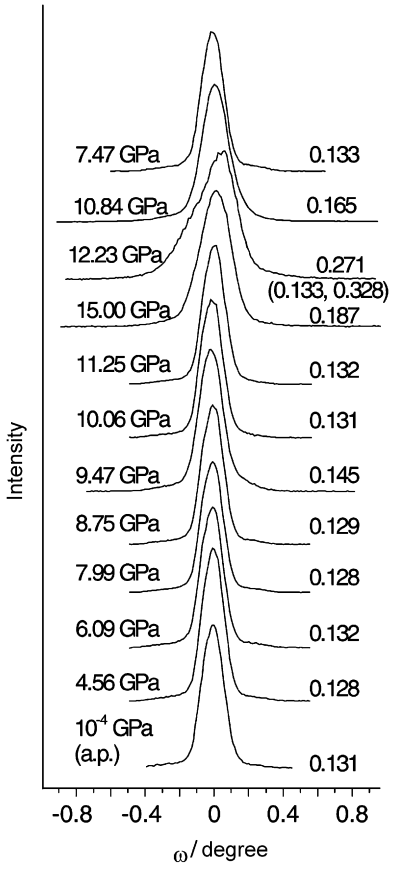

Fig. 2. Line profiles of the reflection 0 0 4 at various pressures. Values in the right side of the line profiles denote the full width at half maximum in ω (deg).

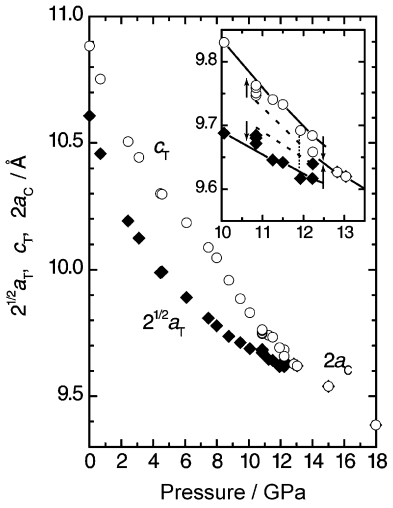

Fig. 3. Pressure dependence of the lattice parameters a_0 and c_0. Error bars are the same as or less than the plotted marks of the data.

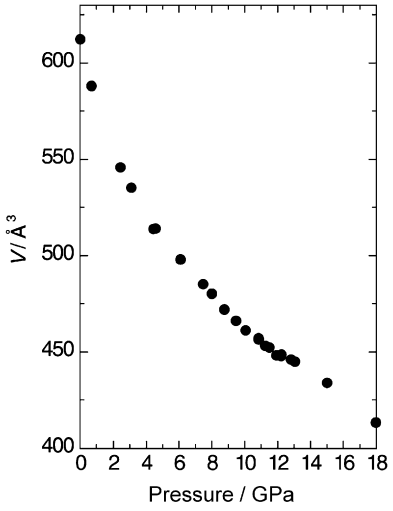

Fig. 4. Pressure dependence of the cell volume. Error bars are the same as or less than the plotted marks of the data.

3. Results

3.1. Pressure dependence of the lattice up to 18 GPa

Lattice parameters a_0 and c_0, and cell volumes of $Cs_2Au_2Cl_6$ determined at 22 different pressures up to 18 GPa are plotted in Figs. 3 and 4, respectively. At 18 GPa, the volume of the original cell at ambient conditions was compressed to 68% compared to the value at ambient conditions. As shown in Fig. 3, $a_{0(L)}$ and $c_{0(L)}$ decrease monotonously with increasing pressure up to ca. 12.5 GPa, where (L) denotes the tetragonal cell setting in a low pressure phase below ca. 12.5 GPa. However, $c_{0(L)}$ exhibits a small anomaly around 8 GPa. The degree of distortion of the tetragonal lattice with respect to cubic symmetry can be expressed by $l_d = 2^{1/2}a_{0(L)}/c_{0(L)}$, the lattice being cubic when $l_d = 1$. The pressure dependence of l_d is plotted in Fig. 5. Tetragonal distortion of the lattice clearly increases with increasing pressure up to ca. 3 GPa when the maximum distortion is reached. Above 3 GPa, the tetragonal distortion decreases. Particularly, above ca. 8 GPa, it abruptly decreases, eventually attaining the point where $l_d = 1$ at ca. 12.5 GPa, i.e. the lattice is cubic as described in the next section.

3.2. Phase transition around 12.5 GPa

As shown in Fig. 3, merging of the $a_{0(L)}$ and $c_{0(L)}$ lattice parameters around 12.5 GPa hints to a phase transition. The increase of $a_{0(L)}$ and decrease of $c_{0(L)}$ result in the relationship $2^{1/2}a_{0(L)} = c_{0(L)}$ ($= 2a_{0(H)}$) at pressures above ca. 12.5 GPa as shown in Fig. 3, the volume of the unit cell remaining more or less unchanged as shown in Fig. 4. This simple relationship concerning the volume of the unit cell may be the reason why the single crystal did not exhibit any twinning or cracking while passing through the transition. The superstructure reflections $h\,k\,l$ (l odd) disappeared above the transition. This implies that the Cl atoms are located at the midpoint between adjacent Au atoms in the high-pressure phase. Fig. 6 illustrates how the intensity of the strongest superstructure reflection, 1 0 3, first decreases in a quasi-linear relationship up to ca. 10 GPa, then

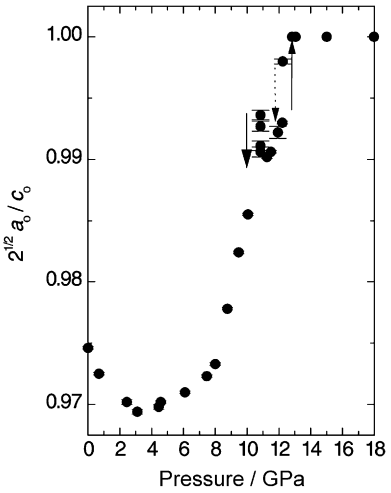

Fig. 5. Pressure dependence of the degree of distortion of the tetragonal lattice with respect to cubic symmetry, $l_d = 2^{1/2}a_{0(L)}/c_{0(L)}$. Error bars are the same as or less than the plotted marks of the data.

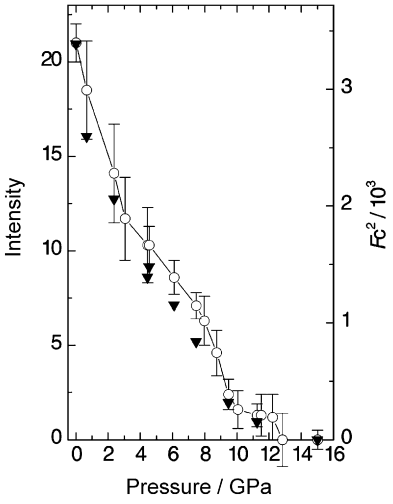

Fig. 6. Pressure dependence of the intensity of the strongest superstructure reflection, 1 0 3. Open circles indicate the intensities observed with the error bars and a broken line as a guide for eyes. Solid triangles indicate the structure factors squared obtained from the refined structures at each pressure.

remains about in a "plateau" before the transition is attained at ca. 12.5 GPa, and finally is vanished above the transition. It is, therefore, concluded that the space group changes at ca. 12.5 GPa from $I4/mmm$ at low pressures to $Pm3m$ at high pressures. The two distinct sites for Au^{I} and Au^{III}, both with tetragonal site symmetries $4/mmm$ in $I4/mmm$ merge to one site with cubic site symmetry $m3m$ in $Pm3m$.

The X-ray diffraction data shows hysteresis behavior between ~10 and ~13 GPa, which is typical for a phase transition of first order, as shown in Fig. 3. It should be noted that in the path of descendant pressure, $2^{1/2}a_{0(L)}$ ($= 2a_{0(H)}$) remained to be almost equal to $c_{0(L)}$ ($= 2c_{0(H)}$) at 12.2 GPa, i.e. the crystal being apparently in the high-pressure phase, while in the path of ascendant pressure, the

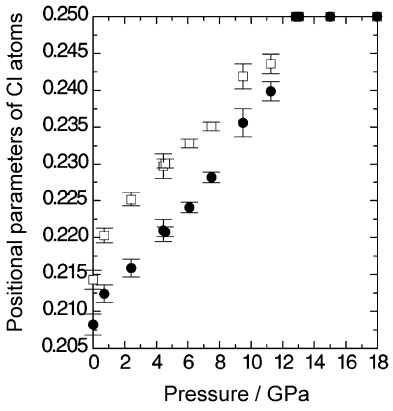

Fig. 7. Pressure dependence of the positional parameters, $x_{Cl(1)}$, $z_{Cl(2)}$ of the Cl atoms. Open squares for Cl(1) and solid circles for Cl(2).

crystal remained to be tetragonal at 12.2 GPa. The crystal at 12.23 GPa in the descendant path was held in the apparent high-pressure phase for 7 days: it remained in a metastable state. Subsequently, it changed to tetragonal symmetry at 10.84 GPa. At 10.84 GPa it was possible to collect distinct sets of cell dimensions for 4 metastable states. Each set was collected over 3 days.

3.3. Crystal structure below the phase transition

The ideally cubic perovskite-type structure does not comprise any free parameter for the atomic positions in addition to the lattice parameter, all atoms being at positions without freedom. The tetragonal perovskite-type structure of $Cs_2Au_2Cl_6$ is described by two positional parameters, $x_{Cl(1)}$ and $z_{Cl(2)}$, Au being at special positions without free parameter. The site symmetries of both Au positions are $4/mmm$, that of Cl(1) is $m.2m$, and that of Cl(2) is $4mm$. Our structure determination using the data collected from the crystal in the high-pressure cell at ambient conditions was in good agreement with that obtained by Eijndhoven and Verschoor [4] without a pressure cell. Positional and isotropic displacement parameters obtained at 11 different pressures are listed in Table 2. The $x_{Cl(1)}$, $z_{Cl(2)}$ parameters and Au–Cl bond lengths are plotted in Figs. 7 and 8, respectively.

The pressure dependencies of $x_{Cl(1)}$ and $z_{Cl(2)}$ as well as bond lengths were found to be quasi-linear, except near ambient pressure. The phase transition is induced when $x_{Cl(1)}$ located in the ab plane and $z_{Cl(2)}$ both reach 0.25, i.e. the midpoint between the nearest Au^{I} and Au^{III} atoms. Consequently the four longer, planar bond lengths in the compressed $[Au^{I}Cl_6]$ octahedron and the two longer, apical bond lengths in the elongated $[Au^{III}Cl_6]$ octahedron are more compressible than the shorter bond lengths, both octahedra eventually attaining regular geometry at the transition.

At low pressures, the octahedra of $[Au^{I}Cl_6]$ and $[Au^{III}Cl_6]$ are significantly distinct. With increasing pressure the dimensions approach each other gradually until they become almost indistinguishable above 12 GPa. The $[Au^{I}Cl_6]$

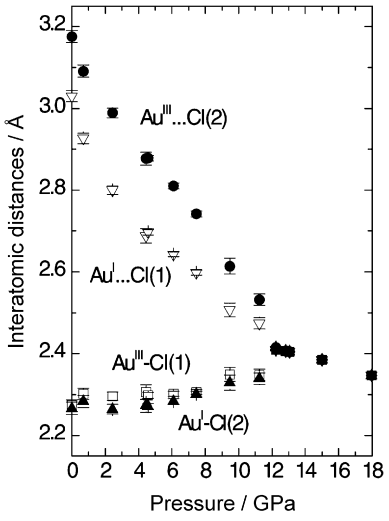

Fig. 8. Pressure dependence of the interatomic distances between the Au atoms and the Cl atoms. Solid triangles, open squares, open anti-triangles, and solid circles indicate the shorter apical distances, Au^{I}–Cl(2) [$= d_a(Au^{I})$], the shorter planer distances, Au^{III}–Cl(1) [$= d_p(Au^{III})$], the longer planer distances, $Au^{I}\cdots$Cl(1) [$= d_p(Au^{I})$], and the longer apical distances, $Au^{III}\cdots$Cl(2) [$= d_a(Au^{III})$] with the error bars, respectively.

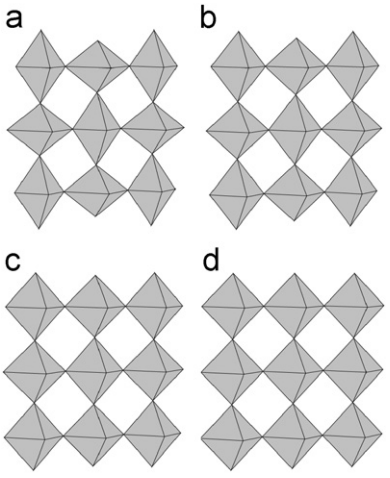

Fig. 9. [$AuCl_6$] octahedra at various pressures: (a) ambient pressure (10^{-4} GPa), (b) 6.09 GPa, (c) 11.25 GPa, (d) 15.00 GPa.

octahedron generally exhibits a somewhat greater volume than the [$Au^{III}Cl_6$] octahedron. The octahedral shapes at 4 different pressures are illustrated in Fig. 9. The pressure dependence of the octahedral volumes and the mean quadratic elongation parameter of Robinson et al. [53], $l = \sum(l_i/l_0)^2/6$ are plotted in Fig. 10. Here, l_0 is the center to vertex distance of the regular octahedron with equal volume, and l_i ($1 \leqslant i \leqslant 6$) are the distances to the six Cl ligands.

In contrast to the generally monotonous pressure dependence of the [$AuCl_6$] octrahedra, the corresponding dependence of the lattice is more complex. For example, the dependence of the distortion parameter l_d ($= 2^{1/2}a_{0(L)}/c_{0(L)}$) is shown in Fig. 5. That parameter includes the effect of the Au–Au distances, i.e. the packing of the ocathedra in addition to the Au–Cl bonds.

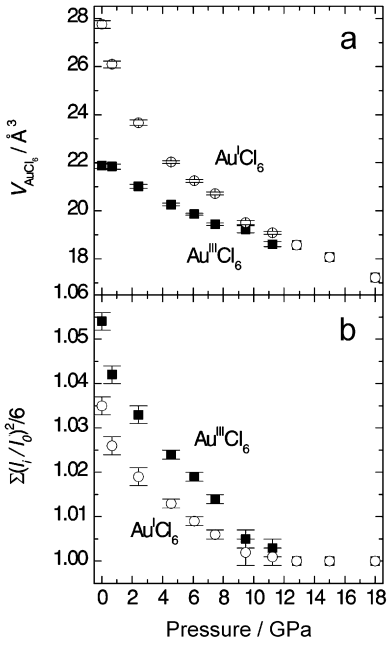

Fig. 10. (a) Pressure dependence of the volume of [$Au^{I}Cl_6$] octahedron and [$Au^{III}Cl_6$] octahedron. (b)Pressure dependence of mean octahedral quadratic elongation parameters. Open circles and solid squares indicate [$Au^{I}Cl_6$] octahedra and [$Au^{III}Cl_6$] octahedra, respectively, in both figures.

3.4. Crystal structure above the phase transition

The relationship between the unit cells of the low pressure phase (L) and the high pressure phase (H) is described by $a_{0(L)}/2^{1/2} = a_{0(H)}$, $c_{0(L)}/2 = c_{0(H)}$, and, at the transition, $2^{1/2}a_{0(L)} = c_{0(L)}$, $a_{0(H)} = c_{0(H)}$. Three-fold axes in the Laue class, of which the existence does not indicate tetragonal but cubic in the present case, were confirmed for the reflections observed at 15 GPa. The confirmation is partial because of a blind region due to the diamond-anvil-cell. A refinement in the tetragonal space group $P4/mmm$ was also attempted but indicated no significant differences from that in the cubic one $Pm3m$ as shown in Table 3. The cubic system has been chosen for the high-pressure phase because of no reason for choosing the lower symmetry.

The diffraction data of the metastable states in the path of descending pressure below 12.5 GPa yielded distinct values for $a_{0(H)}$ and $c_{0(H)}$ ($a_{0(H)} \neq c_{0(H)}$). However, superstructure reflections could not be observed. At any rate, from our present results we cannot derive the existence of a stable, tetragonal $Cs_2Au_2Cl_6$ high-pressure phase reported in the literature [17]. If such a phase does exist at ambient temperature, its phase field, probably around 12 GPa, must be very small.

3.5. Equation-of-state

The isothermal bulk modulus K at zero pressure, K_0, its first pressure derivative, K'_0, and its second pressure derivative, K''_0, are derived by a fourth-order Birch–Murnaghan equation-of-state [54] expressed in

Table 3
Comparison of the refinement of the structure in *Pm3m* with that in *P4/mmm* at 15.00 GPa

Lattice system		Cubic	Tetragonal
Space group		*Pm3m*	*P4/mmm*
Unit cell	a/Å	4.7694(3)	4.7678(4)
	c/Å	$=a$	4.7710(4)
	V/Å^3	108.49(2)	108.46(2)
	Z	1	1
$R[F_o>4\sigma(F_o)]$		0.0195	0.0235
wR		0.0379	0.0453
S		0.763	0.686
No. of reflections used in refinement		47	91
No. of parameters used		5	6
Weighting scheme			
$w=[\sigma^2(F_o)+(aP)^2]^{-1}$ where $P=(F_o^2+2F_c^2)/3$	$a=$	0.0100	0.0100
$(\Delta/\sigma)_{max}$		<0.001	<0.001
$\Delta\rho_{max}$(e/Å^3)		0.63	0.65
$\Delta\rho_{min}$(e/Å^3)		–0.51	–0.91
Au–Cl/Å		2.3847(2)	2.3839(2)[a], 2.3855(2)[b]

[a]In *ab* plane.
[b]Along the *c*-axis.

terms of the Eulerian strain, f, and the Birch normalized pressure,

$$F = K_0[1 + af + bf^2], \quad (1)$$

where the coefficients a, b are

$$a = (3/2)(K'_0 - 4),$$

$$b = (1/6)[9K_0K''_0 + 9K'^2_0 - 63K'_0 + 143].$$

The Eulerian strain, f, is defined by

$$f = [(V/V_0)^{-2/3} - 1]/2 \quad (2)$$

and the Birch normalized pressure, F, is defined by

$$F = P[3f(1+2f)^{2.5}]^{-1}. \quad (3)$$

In Eqs. (2) and (3), P is the pressure, and V and V_0 are the volumes of the unit cell for $Z=4$ at high pressures and at ambient pressure, respectively. The fourth-order Birch–Murnaghan equation-of-state (1) was chosen for the analysis of the isothermal bulk modulus in the present compound, because its unit-cell volume was remarkably compressed down to about 73% around the phase transition point.

The K_0, K'_0 and K''_0 were determined by the least-squares method for the f and F in the Eqs. (1)–(3), using the lattice parameters below the phase transition point. In Fig. 11, the data of the Birch normalized pressure, F as a function of the Eulerian strain, f are plotted and the solid curve shows the quadratic least-squares fit. The intercept of this fit at $f=0$ gives K_0 and the quadratic coefficients a, b give K'_0 and K''_0. The values, $K_0=13(1)$ GPa, $K'_0=10(2)$ and $K''_0=-5(2)$ GPa^{-1} were obtained by the quadratic fit as shown in Fig. 11. Fig. 12 demonstrates the ratio

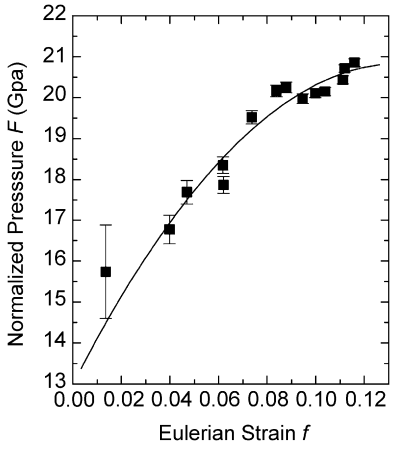

Fig. 11. Experimental pressure dependence of the cell volume as the Birch normalized pressure, F versus the Eulerian strain, f. A solid curve indicates the quadratic least-squares fit.

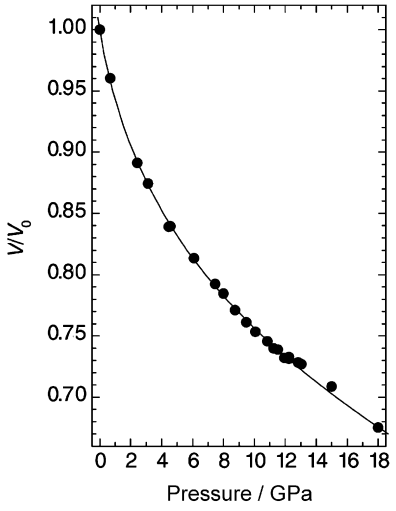

Fig. 12. Pressure dependence of the cell volume based on the fourth-order Birch–Murnaghan equation of state giving the bulk moduli, $K_0=13(1)$ GPa, $K'_0=10(2)$ and $K''_0=-5(2)$ GPa^{-1} (Solid line) and the experimental data (Marks).

of the unit-cell volume, V/V_0 as a function of the pressure, P; the solid line indicates the relation obtained from the values of the bulk moduli. The bulk modulus [$K_0=13(1)$] for $Cs_2Au^IAu^{III}Cl_6$ is much smaller than those of minerals [$K_0=104$ GPa for diopside, $CaMgSi_2O_6$ and $K_0=117$ GPa for hedenbergite, $CaFeSi_2O_6$] [55] and of a perovskite-type oxide [$K_0=104$ GPa for $BaBiO_3$] [56]. That is a little smaller than that of NaCl [$K_0=23.8$ GPa] [54]. Its value is closer to those of organic conductors [from $K_0=9$ GPa for α'-(BEDT-TTF)$_2$Ag(CN)$_2$ to $K_0=13$ GPa for (BEDT-TTF)$_3$CuBr$_4$] [57] rather than the oxides and the chloride.

4. Discussion

As above described, the present compound exhibits the tetragonal-to-cubic transition. The transition pressure of

12.5 GPa is considerably higher than 5.2 GPa claimed by Denner et al. [7]. The apparent discrepancy is to be explained by the development of high-pressure technique using diamond cells with He gas as pressure medium as well as higher precision in measuring diffraction reflections of single crystals. The claimed transition at 5.2 GPa was only an extrapolation based on a small number of measurements with relatively large errors.

Kojima et al. [17] observed a tetragonal to tetragonal transition of $CsAu^{I}Au^{III}Cl_6$ around 12 GPa in powder diffraction patterns. We could not confirm that transition in our single crystal investigation. However, the pressure dependence of the axial ratio $2^{1/2}a_0/c_0$ of the powder study up to 10 GPa is consistent with this present single-crystal data. Our detection of metastable tetragonal states between 10.8 and 12.2 GPa without superstructure reflections, as mentioned in Section 3.4, does not exclude the presence of an intrinsic tetragonal phase field within the region of pressure hysteresis. In the powder study, kerosene was used as a pressure medium. As kerosene is not well hydrostatic under high pressure, a shear stress due to non-hydrostatic condition or pressure anisotropy might be responsible for the appearance of the high-pressure tetragonal phase detected on the powder study.

The remarkable increase of the ratio $2^{1/2}a_0/c_0$ with increasing pressure above 8 GPa, as shown in Fig. 5, may be correlated with the metallization of $Cs_2Au^{I}Au^{III}Cl_6$ around 7.5 GPa [18], suggesting overlap of the HOMO of Au^{I} with the LUMO of Au^{III} above that pressure.

4.1. Au bonding and mixed-valence state in the tetragonal phase

As shown in Fig. 8, the four longer, planar Au^{I}–Cl(1) bonds in the compressed $[Au^{I}Cl_6]$ octahedron and the two longer, apical Au^{III}–Cl(2) bonds in the elongated $[Au^{III}Cl_6]$ octahedron are remarkably compressible. To the contrary, the two shorter, apical Au^{I}–Cl(2) bonds in the compressed $[Au^{I}Cl_6]$ octahedron as well as the four shorter, planar Au^{III}–Cl(1) bonds in the elongated $[Au^{III}Cl_6]$ octahedron slightly elongate with increasing pressure, i.e. those bonds exhibit *negative* compressibility. The distinct, gradual changes of the Au–Cl bond lengths with increasing pressure can be interpreted in terms of "covalency" or "molecular behavior". The Au^{I}–Au^{III} distances between the nearest neighbor of the $[AuCl_6]$ octahedra decrease with increasing pressure, which enhances the intervalence charge–transfer interaction between Au^{I} and Au^{III}. The enhancement of the intermolecular interaction between $[Au^{I}Cl_2]$ and $[Au^{III}Cl_4]$ with increasing pressure weakens the intramolecular bonds of the linear Cl–Au^{I}–Cl bonding and the planar $Au^{III}Cl_4$ bonding in the structure.

Matsushita et al. [6] introduced a parameter δ for estimating the degree of mixed-valence in analogy to a similar parameter used for bridged linear Pt halide complexes [58,59]. For our present case, two such parameters have to be considered: $\delta_p = d_p(Au^{III})/d_p(Au^{I})$ and $\delta_a = d_a(Au^{I})/d_a(Au^{III})$ where d_p refers to the four planar bond lengths and d_a refers to the two apical bond lengths in the $[AuCl_6]$ octahedra. The pressure dependence of δ_p and δ_a is illustrated in Fig. 13. δ_p is greater than δ_a at each pressure below the phase transition. With increasing pressure, δ_p increases almost linearly within the experimental error while the increase of δ_a is not linear and bent around 8 GPa. The significant reduction of the difference $\delta_p - \delta_a$ above about 8 GPa may be related to the onset of semiconductor to metal transition at about 7.5 GPa [18]. There is another aspect of interest: δ_p refers to the bonds within the *ab* plane, whereas δ_a refers to the bonds parallel to the ***c*** axis. Considering the distance between adjacent Au atoms within the *ab* plane in comparison with that parallel to *c*, the intervalence charge–transfer interaction should be enhanced within *ab* compared to that parallel to *c*. The difference of the interaction can give the relation that δ_p is greater than δ_a. Above the phase transition, of course, $\delta_p = \delta_a = 1$. It should be noted that there is an anomaly in the bond lengths at pressures below 1 GPa (see Figs. 7, 8, and 13), which is not yet understood fully.

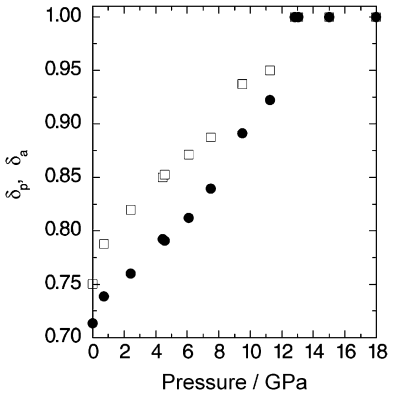

Fig. 13. Pressure dependence of the structural mixed-valence parameters, $\delta_p = d_p(Au^{III})/d_p(Au^{I})$ and $\delta_a = d_a(Au^{I})/d_a(Au^{III})$ where d_p refers to the four planar bond lengths and d_a refers to the two apical bond lengths in the $[AuCl_6]$ octahedra. Open squares and solid circles indicate δ_p and δ_a, respectively.

4.2. Valence state of Au in the cubic phase

Crystallographic equivalency of the Au sites and the regular $[AuCl_6]$ octahedron in the cubic phase above ca.12.5 GPa suggest that all Au atoms exhibit the same electronic state [Xe]$5d^9$: Au^{II}. In general, for a $5d^9$ electronic configuration, Jahn–Teller-type distortion of the $[Au^{II}Cl_6]$ octahedron is expected. In the present case, however, such a Jahn–Teller distortion does not appear.

The conclusion of an intrinsic Au^{II} state in the cubic phase of $CsAuCl_3$ is supported by ^{197}Au Mössbauer spectra of the perovskite $Cs_2Au^{I}Au^{III}I_6$ at high pressures [22]. The spectrum at 12 GPa and at 4.2 K yielded only one state: Au^{II}. The spectrum was a quadrupole-split doublet indicative of distorted $[AuI_6]$ octahdra in $CsAu^{II}I_3$. We are

not aware of any ^{197}Au Mössbauer data of $CsAuCl_3$ above 12.5 GPa.

We have considered the relation of Au^{II} with Jahn–Teller distortion in the present compound in the high-pressure phase in view of the higher-order effect determining the compression or the elongation of Jahn–Teller distortion. In the theory of Jahn–Teller effect [60–62], the first-order coupling terms between the electronic ground state and the lattice distortion cannot yield elongated or compressed octahedra, having two longer, apical bonds and four shorter, planar bonds, or having two shorter, apical bonds and four longer, planar bond, respectively. The higher-order coupling terms yield the distortion pattern. The positive higher-order coupling constant gives the elongated distortion and the negative one gives the compressed distortion. Octahedra elongated by Jahn–Teller effect have been observed in many compounds. On the other hand, compressed octahedra induced by Jahn–Teller effect have been observed only for a few compounds possessing highly electronegative ligands: for example, $KAgF_3$ [63], $CsAgMF_6$ where $M = Sc$, In, Tl [64], and $KCuAlF_6$ [65], and $KCu_3(OH)_2[(As_4)H(AsO_4)]$ [66]. It is expected that such a large distinct of the electronegativity between the central metal and the ligand gives compressed octahedra. The high-pressure phase $CsAu^{II}I_3$ at 300 K is known to be tetragonal with elongated $[Au^{II}I_6]$ octahedra [17]. The Cl, however, is the most electronegative atom in the halogen X for the compounds, $Cs_2Au^{I}Au^{III}X_6$ ($X = Cl$, Br, I). Thus, the $[Au^{II}Cl_6]$ octahedron in the high-pressure phase might be expected to be a compressed one, comparing with $[Au^{II}Br_6]$ or $[Au^{II}I_6]$ ones. As a possible reason for the regular octahedron in the present compound, it is speculated that the $[Au^{II}Cl_6]$ octahedron accidentally become regular as a result of competition between the elongation and the compression of the octahedron caused by the higher-order Jahn–Teller effect.

5. Conclusion

We investigated the detailed crystal structure of $Cs_2Au^{I}Au^{III}Cl_6$ at various pressures up to 18 GPa by single crystal X-ray diffraction method using a diamond-anvil-cell loaded with helium gas as the most ideal inert and hydrostatic pressure-transmitting medium. Pressure dependencies of the lattice parameters and of the cell volume up to 18 GPa has been obtained with reasonable accuracy. The atomic positional parameters of two crystallographically independent kinds of chlorine atom which are the only, variable positional atomic parameters in the structure have been also obtained with accuracy enough to calculate electronic band structures at various pressures. The isothermal bulk modulus at zero pressure [$K_0 = 13(1)$] and its pressure derivatives were obtained from the analysis based on the fourth-order Birch–Murnaghan equation-of-state. We found the structural phase transition from tetragonal ($I4/mmm$) to cubic ($Pm3m$) at ca. 12.5 GPa, associated with the disappearance of the superstructure reflections originated by the shift of the Cl atoms from the midpoint between the Au atoms. The lattice parameters $a_{0(L)}$ and $c_{0(L)}$ discontinuously increased and decreased at the transition point, respectively, resulting in the relationship $2^{1/2}a_{0(L)} = c_{0(L)}$ at pressures above ca. 12.5 GPa. The volume of the unit cell, however, remains more or less unchanged. All the $[AuCl_6]$ octahedra were regular and crystallographically equivalent at pressures above the phase transition. Crystallographic equivalency of the Au sites in the cubic phase above 12.5 GPa suggests that all Au atoms exhibit the same electronic state Au^{II}. Consequently, the structural phase transition is associated with the Au valence transition. The Jahn–Teller distortion expected for the $5d^9$ electronic state of the Au^{II} atom, however, was not apparent. It can be speculated that the $[Au^{II}Cl_6]$ octahedron in the high-pressure phase is accidentally regular as a result of the competition between the elongation and the compression of the octahedron caused by the higher-order Jahn–Teller effect, due to the higher electronegativity of Cl.

Appendix A. Supplementary materials

Supplementary data associated with this article can be found in the online version at doi:10.1016/j.jssc.2007.01.037.

References

[1] J.G. Bednort, K.A. Müller, Z. Phys. B 64 (1986) 189.
[2] R.J. Cava, B. Batlogg, J.J. Krajewski, R. Farrow, L.W. Rupp, A.E. White, K. Short, W.F. Peck, T. Kometani, Nature 332 (1988) 814.
[3] M.B. Robin, P. Day, Adv. Inorg. Chem. Radiochem. 10 (1967) 247.
[4] J.C.M. Tindemans-v Eijndhoven, G.C. Verschoor, Mater. Res. Bull. 9 (1974) 1667.
[5] N. Matsushita, F. Fukuhara, N. Kojima, Acta Crystallogr. E 61 (2005) i123.
[6] N. Matsushita, H. Kitagawa, N. Kojima, Acta Crystallogr. C 53 (1997) 663.
[7] W. Denner, H. Schulz, H. D'Amour, Acta Crystallogr. A 35 (1979) 360.
[8] N. Matsushita, H. Ahsbahs, S.S. Hafner, N. Kojima, Rev. High Pressure Sci. Technol. 7 (1998) 329.
[9] M. Sakata, T. Itsubo, E. Nishibori, Y. Moritomo, N. Kojima, Y. Ohishi, M. Takata, J. Phys. Chem. Solids 65 (2004) 1973.
[10] H. Kitagawa, H. Sato, N. Kojima, T. Kikegawa, O. Shimomura, Synth. Met. 41–43 (1991) 1953.
[11] H. Kitagawa, H. Sato, N. Kojima, T. Kikegawa, O. Shimomura, Solid State Commun. 78 (1991) 989.
[12] P. Day, C. Vettier, G. Parisot, Inorg. Chem. 17 (1978) 2319.
[13] R. Keller, J. Fenner, W.B. Holzapfel, Mater. Res. Bull. 9 (1974) 1363.
[14] N. Kojima, H. Kitagawa, T. Ban, F. Amita, M. Nakahara, Solid State Commun. 73 (1990) 743.
[15] N. Kojima, H. Kitagawa, T. Ban, F. Amita, M. Nakahara, Synth. Met. 41–43 (1991) 2347.
[16] H. Kitagawa, N. Kojima, H. Takahashi, N. Môri, Synth. Met. 55–57 (1993) 1726.
[17] N. Kojima, M. Hasegawa, H. Kitagawa, T. Kikegawa, O. Shimomura, J. Am. Chem. Soc. 116 (1994) 11368.
[18] N. Kojima, F. Fukuhara, H. Kitagawa, H. Takahashi, N. Môri, Synth. Met. 86 (1997) 2175.

[19] M. Katada, Y. Uchida, K. Sato, H. Sano, H. Sakai, Y. Maeda, Bull. Chem. Soc. Jpn. 55 (1982) 444.
[20] H. Kitagawa, N. Kojima, H. Sakai, J. Chem. Soc. Dalton Trans. (1991) 3211.
[21] N. Kojima, F. Amita, H. Kitagawa, H. Sakai, Y. Maeda, Nucl. Instrum. Methods Phys. Res. Sect. B 76 (1993) 321.
[22] S.S. Hafner, N. Kojima, J. Stanek, L. Zhang, Phys. Lett. A 192 (1994) 385.
[23] J. Stanek, S.S. Hafner, H. Schulz, Phys. Lett. A 76A (1980) 333.
[24] J. Stanek, J. Chem. Phys. 76 (1982) 2315.
[25] N. Kojima, H. Kitagawa, J. Chem. Soc. Dalton Trans. (1994) 327.
[26] X.J. Liu, K. Matsuda, Y. Moritomo, A. Nakamura, N. Kojiam, Phys. Rev. B 59 (1999) 7925.
[27] H. Tanino, K. Syassen, Z. Wang, M. Hanfland, K. Takahashi, High Press. Res. 3 (1990) 183.
[28] X.J. Liu, Y. Moritomo, A. Nakamura, N. Kojiam, J. Chem. Phys. 110 (1999) 9174.
[29] X.J. Liu, Y. Moritomo, M. Ichida, A. Nakamura, N. Kojiam, Phys. Rev. B 61 (2000) 20.
[30] H. Tanino, K. Takahashi, Solid State Commun. 59 (1986) 825.
[31] H. Kitagawa, N. Kojima, T. Nakajima, J. Chem. Soc. Dalton Trans. (1991) 3121.
[32] H. Kitagawa, N. Kojima, N. Matsushita, T. Ban, I. Tsujikawa, J. Chem. Soc. Dalton Trans. (1991) 3115.
[33] J.A. Paradis, M.-H. Whangbo, R.V. Kasowski, New J. Chem. 17 (1993) 525.
[34] R. Allub, B. Alascio, Solid State Commun. 85 (1993) 99.
[35] M. Shirai, Synth. Met. 55–57 (1993) 3389.
[36] A.P. Wilkinson, L.K. Templeton, D.H. Templeton, J. Solid State Chem. 118 (1995) 383.
[37] N. Kojima, N. Matsushita, Coord. Chem. Rev. 198 (2000) 251.
[38] N. Kojima, Bull. Chem. Soc. Jpn. 73 (2000) 1445.
[39] L. Merrill, W.A. Bassett, Rev. Sci. Instrum. 45 (1974) 290.
[40] H.K. Mao, P.M. Bell, Carnegie Inst. Washington Year Book 79 (1980) 409.
[41] P. Turk, Dissertation, University of Marburg, Germany, 1989.
[42] H. Ahsbahs, Z. Kristallogr. Suppl. 11 (1996) 30.
[43] L.W. Finger, H. King, Am. Mineral. 63 (1978) 337.
[44] H. King, L.W. Finger, J. Appl. Crystallogr. 12 (1979) 374.
[45] A. Kutoglu, CRYMIS, A Software Package for Structural Analysis (Version 95), University of Marburg, Germany, 1995.
[46] H. Ahsbahs, Prog. Cryst. Growth Charact. 14 (1987) 263.
[47] L. Zhang, H. Ahsbahs, Rev. High Pressure Sci. Technol. 7 (1998) 145.
[48] Stoe and Cie, DIF4, Diffractometer Control Program. Version 7.09.X/DOS, Stoe & Cie, Darmstadt, Germany, 1993.
[49] A. Kutoglu, MDIF4, Diffractometer Control Program for diamond anvil cell. Marburg Version, University of Marburg, Germany, 1995.
[50] D. Naumov, PROFILE, a computing program for the analysis of X-ray diffraction data, Institute of Solid State Chemistry, Novosibirsk, Russia, 1996.
[51] G.M. Sheldrick, SHELXL93, Program for the Refinement of Crystal Structures, University of Göttingen, Germany, 1993.
[52] K. Brandenburg, DIAMOND Version 3.0, Crystal Impact, Bonn, Germany, 2005.
[53] K. Robinson, G.V. Gibbs, P.H. Ribbe, Science 172 (1971) 567.
[54] F. Birch, J. Geophys. Res. 83 (1978) 1257.
[55] L. Zhang, H. Ahsbahs, S.S. Hafner, A. Kutoglu, Am. Mineral. 82 (1997) 245.
[56] T. Hashimoto, N. Matsushita, Y. Murakami, N. Kojima, T. Kikegawa, H. Kawazoe, unpublished result.
[57] P. Guionneau, J. Gaultier, D. Chasseau, G. Bravic, Y. Barrans, L. Ducasse, D. Kanazawa, P. Day, M. Kurmoo, J. Phys. I France 6 (1996) 1581.
[58] M. Tanaka, I. Tsujikawa, K. Toriumi, T. Ito, Acta Crystallogr. C 42 (1986) 1105.
[59] N. Matsushita, K. Toriumi, N. Kojima, Mol. Cryst. Liq. Cryst. 216 (1992) 201.
[60] U. Öpik, M.H.L. Pryce, Proc. R. Soc. A 238 (1957) 425.
[61] A.D. Liehr, C.J. Ballhausen, Ann. Phys. 3 (1958) 304.
[62] M.H.L. Pryce, K.P. Sinha, Y. Tanabe, Mol. Phys. 9 (1965) 33.
[63] R.H. Odenthal, R. Hoppe, Monatsh. Chem. 102 (1971) 1340.
[64] B.G. Müller, J. Fluorine Chem. 17 (1981) 317.
[65] G. Wingefeld, R. Hoppe, Z. Anorg. Allg. Chem. 516 (1984) 223.
[66] H. Effenberger, Z. Kiristallogr. 188 (1989) 43.